This is a non-peer reviewed EarthArXiv preprint

**This is an EarthArXiv preprint that has not undergone peer-review.**

**We welcome comments and suggestions through email.**

This is a non-peer reviewed EarthArXiv preprint

# Fluid invasion dynamics in porous media with complex wettability and connectivity

Arjen Mascini[1,2], Marijn Boone[3], Stefanie Van Offenwert[1,2], Shan Wang[1,2], Veerle Cnudde[1,2,4] & Tom Bultreys[1,2]

[1] Pore-scale Processes in Geomaterials Research Team (PProGRess), Department of Geology, Ghent University Krijgslaan 281/ S8, 9000 Ghent, Belgium, e-mail: Arjen.Mascini@UGent.be

[2] Centre for X-ray Tomography (UGCT), Ghent University, Proeftuinstraat 86, 9000 Ghent, Belgium

[3] TESCAN XRE, Bollebergen 2B box 1, 9052 Ghent, Belgium

[4] Department of Earth Sciences, Utrecht University, Princetonlaan 8a, 3584 CB Utrecht, The Netherlands.

Author contribution: A.M., V.C., and T.B. designed research; A.M., M.B., S.V.O., S.W., and T.B performed research; A.M., and S.V.O. analyzed data; A.M. and T.B wrote the paper with input from the other co-authors.

Key words: X-ray computed microtomography, Heterogeneous porous media, Pore-scale imaging, Wettability, Capillarity

## Abstract

Fluid invasion into porous materials is very common in natural and industrial processes. The fluid invasion dynamics in simple pore networks are governed by a global balance of capillary, viscous and inertial forces. However, significant local variability in this balance may exist inside natural, heterogeneous porous materials. Here, we imaged slow fluid intrusion in two sister samples of a heterogeneous sandstone, one water-wet and one mixed-wet, using high-resolution 4D X-ray imaging. The pore-by-pore fluid invasion dynamics were quantified, revealing a new type of mixed-wet dynamics where 19% of the fluid invasions were orders of magnitude slower than in directly neighboring pores. While conventional understanding predicted strongly capillary-dominated conditions, our analysis suggests that viscous forces played a key role in these dynamics, facilitated by a complex interplay between the mixed-wettability and the pore structure. These previously unknown dynamics highlight the need for further studies on the fundamental controls on multiphase flow in complex natural porous materials, which are abundant in e.g. groundwater remediation and subsurface $CO_2$ storage operations.

## Introduction

The simultaneous flow of multiple fluid phases through a porous material is an important process encountered in many natural and manmade systems. Multiphase flow plays a crucial role in transport in fuel cells (1), safe medical facemasks (2) and self-cleaning materials (3). In earth sciences, it is critically important for the injection and safe storage of $CO_2$ in deep saline aquifers (4), geological energy storage (5) and the study of subsurface contaminant transport (6).

The pore-scale dynamics of multiphase flow in porous media are known to be governed by a competition between the driving forces on the fluids: capillary, viscous, inertial forces (gravitational forces are generally considered negligible at the pore scale) (7–10). These dynamics determine how fluids occupy the available space in the pores and how the resulting fluid distribution evolves over time. For example, an invading fluid can form a flat front, steadily displacing the defending fluid, or it can form ramified "fingers" penetrating into the defending fluid (10). Fluid invasion in 2D networks was found to have qualitatively different properties when the injection flow rate or fluid properties were varied (11, 12), resulting in a "phase diagram" of flow regimes in function of the capillary number (average ratio of viscous to capillary forces) and the viscosity ratio of the two fluids. The development of these pore-scale fluid arrangements into distinct patterns has a crucial impact on the macroscopic transport behavior, yet continues to challenge our pore-scale models (13).

A particular problem has been the understanding of how pore-scale variations in the pore geometry and the wettability (the relative affinity of the fluids to the solid surface) affect fluid intrusion in porous materials. Recently, Lenormand's phase diagram was extended to incorporate random disorder (7) and the influence of homogeneous wetting conditions in 2.5D micro-models (10, 14). However, natural materials such as porous rocks, sediments and soils frequently exhibit much higher degrees of correlated disorder ("heterogeneity"), with pore sizes spanning many orders of magnitude (15). Furthermore, the effective wettability in the pores of geological materials is subject to variations in mineral composition and surface roughness at all length scales (16, 17), and can be impacted by coatings of surface-active components, particularly in hydrocarbon reservoirs (18) and polluted aquifers (19). This can lead to different surfaces having a different fluid affinity, commonly referred to as "mixed-wettability" (20, 21), which also occurs in other natural phenomena such as self-cleaning lotus leaves (22) and antifogging mosquito eyes (23). Multiphase flow has spatial dependencies that stretch over many pores, and consequently it is still poorly understood how pore-scale heterogeneities influence the fluid invasion dynamics. Nevertheless, their importance is critical in groundwater (6), energy (5) and carbon storage technologies (4).

To study the fluid invasion dynamics in complex porous media, time-resolved high resolution X-ray microtomography (mCT) can be applied to image the fluids' distribution in the pores at the second to minute time scale in three dimensions (24, 25). This technique led to the first observations of capillary-dominated fluid displacement events in rock samples (26–28) and of complex dynamic effects such as ganglion dynamics (29) and intermittency (30). Despite this significant progress, most time-resolved imaging has been performed on rocks with essentially single-scale pore structures, and the dynamics in such samples exhibiting heterogeneous wettability have only recently started to be studied (31, 32). Furthermore, most studies have focused on describing the geometry and connectivity of the fluids during displacements and in the resulting fluid distributions, while the time scales associated with the dynamics received relatively little attention (33). This leaves unanswered whether the current knowledge on capillary-dominated fluid dynamics covers the behavior that typically occurs in the subsurface.

In this work, the pore-scale dynamics of capillary-dominated multiphase flow are investigated in microcores of a heterogeneous sandstone in both homogeneously water-wet and mixed-wet conditions. The time scales of fluid displacements are estimated on a pore-by-pore basis using time-resolved laboratory-based X-ray mCT to image the fluid distribution in the pores. We show that the dynamics were qualitatively different in mixed-wet conditions and in water-wet conditions. Under mixed-wet conditions, an important fraction of the pores had fluid displacement time scales that were several orders of magnitude slower than directly neighboring pores. These slow dynamics appeared to be dominated by the fluid conductivity rather than by capillary forces (despite the low capillary number). This implies that in complex porous media, flow regimes commonly thought to be controlled by capillary forces may in fact digress significantly from this assumption. This puts into question the use of classical concepts such as the capillary number to characterize multiphase flow.

## Results and discussion

To investigate fluid dynamics in complex porous media, we performed unsteady-state multiphase flow experiments in two twin microcores of a heterogeneous, calcareous Luxembourg Sandstone (34) with a multiscale pore geometry. One sample was used in its native homogeneously hydrophilic (water-wet, WW), state, while the wettability of the second sample was chemically altered to obtain a mixed-wettability (MW) to water and oil. We performed oil- (OF) and subsequent water flooding (WF) experiments using a KI-brine as watery phase and decane as oil phase. The experiments were imaged continuously using dynamic laboratory-based mCT (TESCAN DynaTOM scanner) with imaging temporal resolutions of 60 seconds (WW-OF, MW-WF) and 120 seconds (WW-WF) per image and a voxel size of 8 µm. The dynamic imaging was supplemented with higher spatial and temporal resolution imaging prior to and after each experiment. Further details can be found in the Material and Methods section and Supporting Information.

In the water-wet sample the oil flood was a drainage process, as decane is the non-wetting phase intruding the sample, and similarly the water flood was an imbibition. To mimic flow in the subsurface, the fluid flux in the experiments was very low, with capillary numbers ($C_a$ =

μv/σ, where υ the characteristic fluid velocity in the pores, μ the invading fluid's viscosity and σ the interfacial tension) on the order of $10^{-8}$, so that capillary forces would typically be assumed to dominate. Theoretically, we therefore expected to find three types of irreversible, fast pore filling "events" on the millisecond time scale: piston-like displacement (e.g. Haines jumps during drainage), snap-off, and cooperative pore filling (35, 36). These events were anticipated to be interspersed with reversible interface movements (e.g. wetting layer swelling) on the time scale of seconds to hours (33). Below, we first qualitatively compare our experimental results to this conventional picture. Then, the timescales and flow rates are quantified on a pore-by-pore basis. Next, the role of wettability on the displacements is investigated. Finally, the viscous-capillary force balance of the observed dynamics is investigated.

**Qualitative comparison of displacement processes**

Under water-wet conditions, oil was observed to displace the watery phase in a sequence of large meniscus jumps (Movie S1). These jumps were significantly faster than the temporal resolution of the mCT imaging, thus appearing as instantaneous pore-scale displacement events in the mCT images. This is conform the expectation that the drainage process takes place as an intermittent sequence of Haines jumps at the milli-second time scale (35). In the subsequent water flooding experiment (Movie S2), water layers were observed to slowly swell from the sides of the pores (Figure S6), causing the oil to become disconnected by the occurrence of sudden snap-off events in narrow constrictions of the pore space. This behavior is typical for imbibition in a water wet medium with a high pore-throat aspect ratio (37), and led to significant non-wetting phase trapping of the oil.

The sample with a mixed-wettability showed a notably different behavior (Figure 1; Movie S3) during water flooding. The majority of the displacements were filled in fast events comparable to the drainage process in the water-wet sample. However, three observations stood out. First, the front at which the displacements occurred was more compact than that of the water-wet drainage case (Figure S7). Second, a significant part of the pores changed fluid occupancy over a much slower time scale: it took tens of minutes rather than a single time step for a fluid meniscus to move through such a pore. The slow events occurred concurrently with the fast events in neighboring pores. They typically happen in poorly connected moldic pores, that often appear to be only connected to the rest of the network by micropores below the imaging resolution. Third, the pore walls of many of these pores visually appeared to be partly water-wet and partly oil-wet (Figure 1). We observed both events where water moved into the center of the pore body while bulging into the oil (Figure 1 event 1; Figure 2; Movie S4-5) and events with a near flat meniscus (Figure 1, event 2; Movie S6-7). This was distinct from layer swelling during water flooding of the water-wet sample, where the water-layers always swelled from the smaller pores and corners.

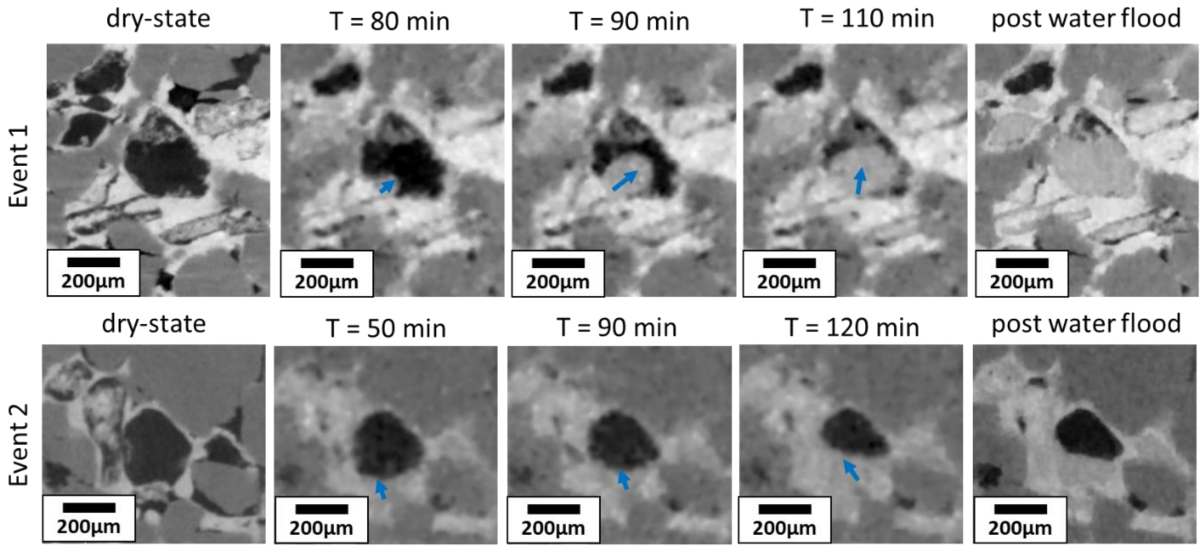


***Figure 1*** *Visual comparison of two "slow" events show different fluid configurations of water (light grey) and oil (black). The blue arrows indicate the movement of the watery phase. During event 1 water is observed to bulge into the oil-phase indicating oil-wet conditions. In contrast, oil bulges weakly into the watery phase during event 2 indicating weakly water-wet to intermediate wetting conditions.*

**Quantifying the time scales of pore-scale displacements**

To quantify the times scales of individual pore-scale displacements, the pore space was divided into pore bodies separated at local constrictions (38). The change in fluid saturation of each pore body over time was calculated by counting the number of segmented oil voxels within their volume. The duration of a fluid displacement event (Figure 2) was found by identifying the start and finish times of the saturation change in a pore body, and calculating the transient time during which the oil saturation in it increased or decreased (limited by the temporal resolution of the imaging). Pores that changed occupancy with less than 10% were omitted from the analysis to lower the influence of image noise.

In the water-wet sample, 98% of the displaced volume during the oil flood was associated with pore filling events that completed faster than the temporal resolution of the imaging (Figure 3a). Longer pore filling events were associated with two or more intermittent displacements inside one pore body that each took less than one time step to complete. Displacements during the water flood in the same sample took typically 10-20 min to complete (Figure 3a). Note that the filling duration calculated here included the reversible swelling of wetting layers, which led up to capillary instabilities and subsequent "snap-off" redistributions of the fluids.

The displacements in the MW-WF case had a distinctively different temporal signature. While most of the fluid displacement occurred in events that took less than one time step to complete, 19% of the displaced oil volume was associated with events that took longer than 60 seconds. The cumulative pore filling duration distribution shown in Figure 3a has a long tail, spanning almost the full duration of the experiment. These slow fillings appeared not to be dominated by capillary forces in the same way as during a typical drainage, which would have resulted in instabilities that caused fast fluid redistribution as soon as the invasion capillary pressure of a pore throat was overcome. Displacements with a long duration occurred concurrently with those that completed within one time step, as can be seen in Figure 3b, which shows the start and finish time of each detected displacement event. The slow filling dynamics may therefore have a non-trivial influence on the order in which pores are invaded by brine, and therefore potentially on the fluid distribution patterns that arise from this.

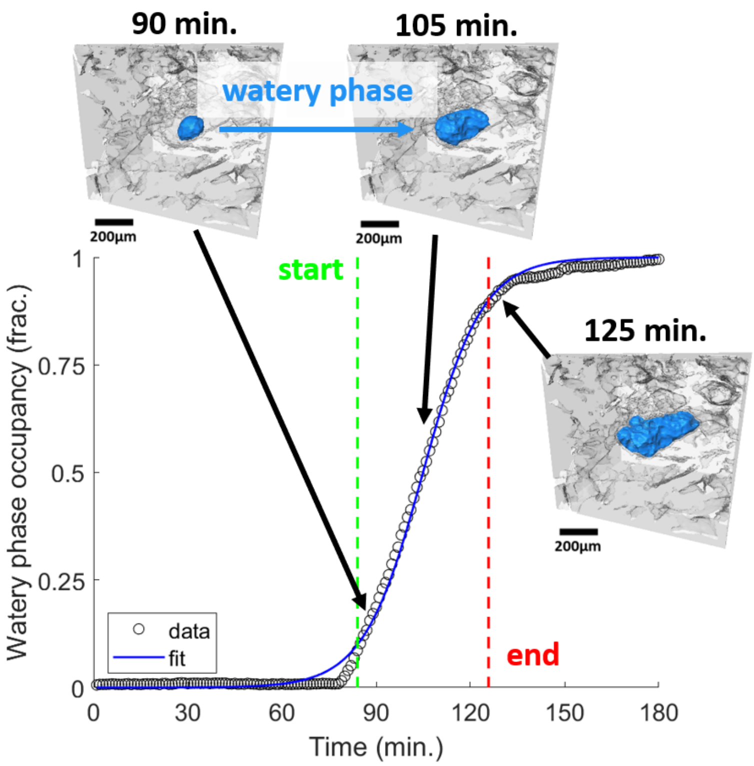


***Figure 2*** *By calculating the fluid occupancy over time for a single pore body, displacements can be identified and the duration of the event be calculated.*

**Displacement efficiencies**

The fluid distributions (and thus the upscaled properties such as the relative permeability) after a displacement are influenced by the efficiency of the displacement process. In a piston-like displacement, the wetting phase can theoretically displace all of the non-wetting phase. In contrast, snap-off leaves behind more non-wetting phase, as the latter becomes disconnected and may therefore be trapped in the pore-space.

The displaced fraction (watery phase for oil flood, oil-phase for water flood) was quantified using the difference in oil-saturation of each pore before and after a displacement event was detected (Figure 3c). The drainage process observed in the WW sample was highly efficient, displacing most of the resolved watery phase. Small amounts of water were left behind in corners, surface roughness and microporosity. The imbibition process in the same sample was much less efficient and typically only displaced 20% of the oil-phase in pore bodies where an event was detected, leaving as much as 80% percent behind.

The water flooding in the MW sample was found to be even more efficient than the drainage process in the WW sample, highlighting the importance of the role of surface wetting on the overall displacement processes. It also clearly shows the distinction between the slow events in the water-wet water flooding (due to layer swelling) and the slow invasion events in the mixed-wet water flooding, which tended to invade the pore centers in a piston-like manner.

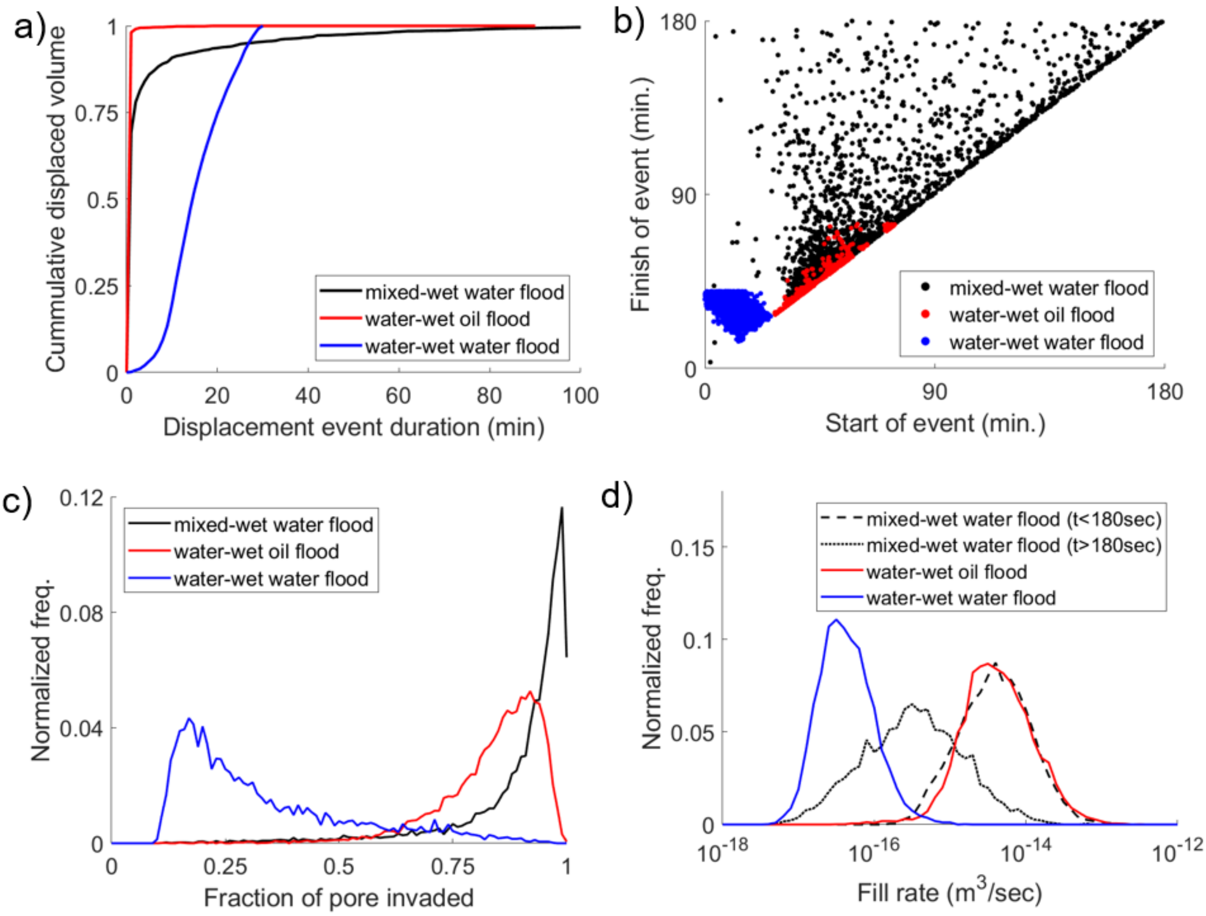


***Figure 3 a)*** *During the water flood in the altered wet sample more than 19% of the total displaced volume of fluid occurred in events that took more than a minute to complete.* ***b)*** *Start and finish times were identified on a pore-by-pore basis.* ***c)*** *The displacement efficiency clearly shows the difference between water flood during water-wet and mixed-wet conditions.* ***d)*** *Distribution of effective fill rates for fluid displacement events in individual pores. This figure includes events that occur at time scale faster than the temporal resolution of the imaging. In those cases,* *the calculated effective filling rate is a lower limit and is likely much higher. Events with a duration shorter than 180 seconds are plotted separately from those who took more than 180 seconds to complete.*

## Effective displacement rates

The rate at which fluids flow through a porous medium is closely related to the capillary-viscous force balance that control the fluid distributions. We investigated this by defining the effective displacement rate as the volume of displaced fluid divided by the filling duration. The calculated effective displacement rates are shown in Figure 3d. These are a lower limit to the actual displacement rates due to the limited temporal resolution of the measurement. Note that the effective filling rates for a single pore were up to six orders of magnitude slower than the overall flow rate set on the pump ($1 \cdot 10^{-11}$ $m^3$/sec).

## Wettability and pore scale dynamics

Wettability has a strong influence on the position of the fluid-fluid interfaces during multiphase flow and can alter the sequence in which pores are invaded in mixed-wet media (32). The wettability of a material is quantified by a contact angle, that can be calculated geometrically directly from 3D mCT images of fluid distributions (39). Contact angles were calculated on high-resolution images of the static fluid distributions after water flooding and are presented in Figure 4 for both samples. The mean contact angle for the sample in its native state was 68.5°, indicating weakly-water wet conditions. The MW sample had a mean of 93.9° with part of the distribution below and above 90°, indicating mixed-wet conditions (20). The width of the contact angle distributions can be attributed in part to the dynamics of the fluid-fluid interface (40) as well as artefacts related to limited spatial resolution (41).

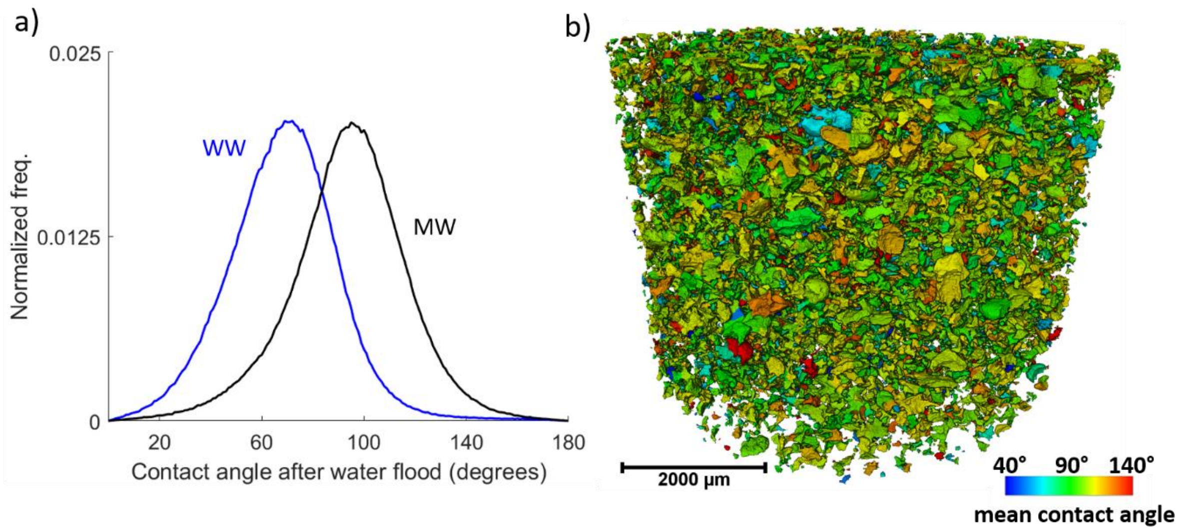


***Figure 4 a)*** *Distributions of contact angles on static fluid distributions after the water flood. The mixed-wet distribution shows a distribution that covers both values above and below 90 degrees which is typical for mixed-wet* *rocks.* ***b)*** *The spatial distribution of contact angles post water flood averaged for each pore body inside the mixed-wet sample.*

By themselves, the measured wettability properties of the mixed-wet sample did not explain the slow filling dynamics that we observed. In addition to the "static" contact angles in Figure 4, we investigated the relation between the wettability and the dynamics by measuring the local contact angles at the start of each fluid invasion event in the dynamic imaging data (40). Unlike contact angle measurements on static fluid distributions, which contain pinned contact lines that can yield any value between the advancing and receding contact angles, the latter "event-based" measurements indicate the advancing contact angle at the time when fluid displacements started (Figure 5a). In our mixed-wet experiment, the event-based contact angles were very similar in fast- and slow-filling pores, as was the hysteresis between the measured contact angles at the start and end of the filling events (Figure 5b). This suggests that the time-scale of the dynamics was not controlled by the local wettability alone. Nevertheless, contact angle measurements on fast time resolved mCT data may suffer from the limited spatial and temporal resolution of these measurements, and further experiments with higher resolutions are needed to confirm this.

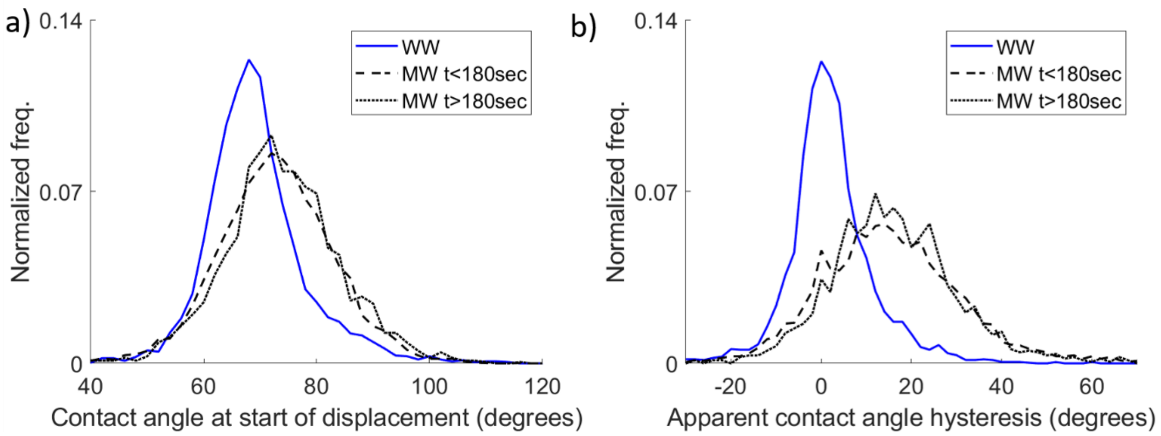


***Figure 5 a)*** *Distribution of the mean contact angles for each pore body at the start of the displacement event calculated on the dynamic mCT data of the water- and mixed-wet data.* ***b)*** *Distribution of the apparent contact angle hysteresis per pore for both water- and mixed-wet conditions during water flooding. In both a) and b) there is no obvious difference in distribution between events that take less than 180 seconds and events that take longer to complete.*

## Filling dynamics and the viscous-capillary force balance

In the capillary limit, fluid displacement can only take place if both fluid phases are connected through the sample (i.e. there is no mobilization of trapped ganglia due to viscous forces). When connected fluid pathways become narrow, the area available for fluid flow may limit the rate of fluid displacements. Conductivity-limited behavior has been observed indirectly during the final stages of drainage experiments in water-wet rocks (42). During these final stages, the water phase is displaced via a network of thin water layers in the corners and crevices of rough pore walls. As the area available for the water phase is limited, the relative permeability is very low (orders of magnitude lower than the relative permeability of the non-wetting phase). The time it takes to reach capillary equilibrium in this case can be days for a small cm-scale sample, compared to the timescale of milliseconds of the initial Haines jumps that filled most of the pore space (43). There are however important differences with the fluid filling events described in this work: the events here happen concurrently with the fast displacements occurring in neighboring pores and fill complete pore bodies rather than consisting of interfaces merely invading small pore corners and crevices. They therefore have the potential of severely impacting the displacement sequence, and thus the upscaled flow properties.

The prevalence of the slow filling events can be explained by taking into account both the wettability and the pore space architecture. Microporous materials such as mineral cements and clays can provide structural bottle necks between larger intergranular pores that impede fluid flow. The pore throats in these narrow structures might differ orders of magnitude with larger neighboring pores. Large heterogeneity in the pore size promotes the loss of fluid connectivity during the invasion, due to trapping by e.g. snap-off and bypassing (43). However, mixed-wet systems are known to preserve this connectivity longer than homogeneously-wetted systems (44). As a consequence, filling events that cannot proceed in a water-wet systems, may proceed in mixed-wet systems. When this happens, narrow connections through micro-pores and wetting layers therein may cause bottlenecks in the fluids' "supply chain", thereby causing conductance-limited behavior which significantly slows down the pore-scale invasion dynamics. This likely explains why slow filling dynamics were less pronounced in previous studies of mixed-wet systems with simpler pore structures, such as Bentheimer sandstone or Ketton limestone (31, 32).

The local balance between viscous and capillary forces during the slow filling events can be investigated using a simple model of the pore space architecture in our experiment. Mercury intrusion porosimetry (Figure S1) showed that the sample had a bimodal pore throat size distribution centered on throat radii $R_{micro}$ = ~2 µm and $R_{inter}$ = ~20 µm for the micro- and intergranular pores respectively. We model the situation that the invading fluid had to pass through a patch of tight throat radii to invade a large pore. The flow thus passed through an intergranular pore (throat) with typical dimensions on the order of $R_{inter} \times R_{inter} \times R_{inter}$, which was cemented with microporous material with throat size $R_{micro}$. Using respectively the multiphase extension of the Darcy equation and the Young-Laplace equation, the balance between the viscous pressure drop $P_v$ over this blocked throat and its capillary intrusion pressure $P_c$ is:

$$\frac{P_v}{P_c} = \frac{\mu q_{local} R_{inter}}{k_{micro} \cdot k_{micro,r}} \cdot \frac{R_{micro}}{2\sigma\,|\cos\theta|} = Ca_{local} \cdot \frac{R_{micro} \cdot R_{inter}}{k_{micro} \cdot k_{micro,r}} \cdot \frac{1}{2\,|\cos\theta|}$$

Where μ is viscosity, $q_{local}$ is the local fluid flux approximated by the effective displacement rate, $k_{micro}$ and $k_{micro,r}$ are the absolute and relative permeability of the microporosity, σ is the interfacial tension, θ is the advancing contact angle and $Ca_{local}$ is a local capillary number defined to equal $\mu q_{local}/\sigma$. Following (43), a typical permeability for the microporosity with this throat size is on the order of $10^{-15}$ $m^2$, and the average contact angle was 93.5° (Figure 4). Filling in these values, we find that:

$$\frac{P_v}{P_c} \approx 10^5 \cdot \frac{Ca_{local}}{k_{m,r}}$$

Based on the flow rates measured in the mCT data, the typical $Ca_{local}$ for slow pore filling events mediated by this microporous patch would be on the order of $10^{-7}$ (Figure S8). Given the fact that the relative permeability to either the invading or the escaping phase is expected to be low ($<<10^{-1}$) in a mixed-wet medium, the local ratio between viscous and capillary forces can easily approach values on the order of 1. This indicates that in samples where pore sizes differ orders of magnitude, viscous forces could play a significant role in the displacement process even at very low global capillary numbers. The mixed-wet wettability plays a crucial role here, as it allows to maintain fluid connectivity – and thus displacement processes to proceed – even for very low relative permeabilities to either of the fluids.

## Conclusions

To investigate multiphase flow dynamics in porous materials with a complex pore structure and wettability, we used time-resolved microcomputed tomography to image unsteady-state multiphase flow experiments in two microcores of a calcareous sandstone. The pore-scale dynamics are shown to be qualitatively and quantitative different for samples in the water- and mixed-wet conditions. We identified a novel displacement mechanism during water flood under mixed-wet conditions where a significant part of the pores change fluid occupancy at time scales which are orders of magnitude slower than those of directly neighboring pores. These observations indicate that even at low capillary numbers, viscous forces can influence the displacement process in complex pore spaces, particularly under mixed-wet conditions.

One of the main open questions in the field of multiphase flow is how to link pore-scale displacements to macro-scale behavior of multiphase flow described by continuum-scale equations. Most continuum descriptions implicitly assume static fluid distributions for constant flow conditions. However, multiphase flow is a dynamic process: the fluid patterns are not stable and no genuine steady state exists. This has been demonstrated experimentally for higher capillary numbers ($10^{-6}$-$10^{-4}$), in the form of intermittency (30), ganglion dynamics (29) or break-up of ganglia in rocks with a multiscale pore system (45). The work presented here demonstrates that even at much lower capillary numbers (~$10^{-8}$), pore-scale complexities such as mixed-wettability and multi-scale pore geometries can cause significant pore-scale variations in the capillary-viscous force balance. This gave rise to previously undescribed pore-scale dynamics that may contribute significantly to the overall volume and order of the pore-scale fluid displacements, and thus to the macro-scale behavior. Our observations of these dynamics spurs further investigation into the classification of phenomena caused by pore-scale variability in the driving forces of multiphase flow in heterogeneous porous materials. Ultimately, this may lead to better models of fluid flow in the subsurface critical for groundwater resources and $CO_2$ sequestration operations.

## Materials and Methods

Unsteady-state core flooding experiments were performed using a 1.0 mol·$kg^{-1}$ potassium iodide (KI) brine as watery phase and n-decane as oil phase, a flow rate of 0.0006 ml/min and at ambient temperatures. The fluid viscosities were taken to be $\mu_{brine}$ = 0.82 mPa/s and $\mu_{decane}$ = 0.84 mPa/s and an interfacial tension of 52 mN·$m^{-1}$ (46–48). Under these conditions, the macroscopic capillary number for the flooding experiments was $3 \cdot 10^{-8}$.

Two 29 mm long, 6 mm diameter microcores of Luxembourg Sandstone (Carrières Feidt Ernzen, Luxembourg) were used: one in its native water-wet state, while the wettability of the second sample was chemically altered by partial liquid phase deposition of Octadecyltrichlorosilane (OTS) rendering it mixed-wet (49).

The sample was mounted in an X-ray transparent core holder with a confining pressure of 3.65MPa. The experiments were imaged using a TESCAN DynaTOM scanner (TESCAN, Czech Republic). mCT scans were acquired continuously during the experiments (8 µm/vx) and higher resolution imaging (4 µm/vx for WW and 3.5 µm/vx for MW) was performed prior to and after each flooding experiment.

Each image in the time series was processed and segmented using Avizo 2020.2 (Thermo Fisher Scientific) to classify voxels in each image either belonging to mineral, oil or watery phase (50). Filling times were calculated by fitting a sigmoidal function to the normalized pore occupancy data (51). Contact angles were calculated using an automatic method (39).

A more detailed description of materials and methods is provided in Supporting Information.

## Acknowledgements

We would like to thank TESCAN XRE for the access to their DynaTOM system and their support during the experiments. This research received funding from the Research

Foundation–Flanders (FWO, project G051418N). Tom Bultreys is a postdoctoral fellow of the Research Foundation–Flanders (FWO) and acknowledges its support under grant 12X0919N. Sorin Pop, Carina Bringedal and Stephan Lunowa are thanked for their insightful discussions that helped to give shape to this work. The imaging data can be retrieved from https://www.digitalrocksportal.org/.

## References

1. R. Borup, *et al.*, Scientific Aspects of Polymer Electrolyte Fuel Cell Durability and Degradation. *Chem. Rev.* **107**, 3904–3951 (2007).
2. Y. Li, *et al.*, In vivo protective performance of N95 respirator and surgical facemask. *Am. J. Ind. Med.* **49**, 1056–1065 (2006).
3. R. Blossey, Self-cleaning surfaces — virtual realities. *Nat. Mater.* **2**, 301–306 (2003).
4. M. Bui, *et al.*, Carbon capture and storage (CCS): the way forward. *Energy Environ. Sci.* **11**, 1062–1176 (2018).
5. J. Mouli-Castillo, *et al.*, Inter-seasonal compressed-air energy storage using saline aquifers. *Nat. Energy* **4**, 131–139 (2019).
6. J. W. Mercer, R. M. Cohen, A review of immiscible fluids in the subsurface: Properties, models, characterization and remediation. *J. Contam. Hydrol.* **6**, 107–163 (1990).
7. R. Holtzman, Effects of Pore-Scale Disorder on Fluid Displacement in Partially-Wettable Porous Media. *Sci. Rep.* **6**, 36221 (2016).
8. R. Hu, T. Lan, G.-J. Wei, Y.-F. Chen, Phase diagram of quasi-static immiscible displacement in disordered porous media. *J. Fluid Mech.* **875**, 448–475 (2019).
9. R. Lenormand, C. Zarcone, A. Sarr, Mechanisms of the displacement of one fluid by another in a network of capillary ducts. *J. Fluid Mech.*, 337–353 (1983).
10. B. Zhao, C. W. MacMinn, R. Juanes, Wettability control on multiphase flow in patterned microfluidics. *Proc. Natl. Acad. Sci.* **113**, 10251–10256 (2016).
11. M. J. Blunt, H. Scher, Pore-level modeling of wetting. *Phys. Rev. E* **52**, 6387–6403 (1995).
12. R. Lenormand, E. Touboul, C. Zarcone, Numerical models and experiments on immiscible displacements on immiscible displacements in porous media. *J. Fluid Mech.*, 165–187 (1988).
13. B. Zhao, *et al.*, Comprehensive comparison of pore-scale models for multiphase flow in porous media. *Proc. Natl. Acad. Sci.* **116**, 13799–13806 (2019).
14. M. Trojer, M. L. Szulczewski, R. Juanes, Stabilizing Fluid-Fluid Displacements in Porous Media Through Wettability Alteration. *Phys. Rev. Appl.* **3**, 054008 (2015).
15. M. J. Blunt, *et al.*, Pore-scale imaging and modelling. *Adv. Water Resour.* **51**, 197–216 (2013).

16. P. G. de Gennes, Wetting: statics and dynamics. *Rev. Mod. Phys.* **57**, 827–863 (1985).

17. N. R. Morrow, The Effects of Surface Roughness On Contact: Angle With Special Reference to Petroleum Recovery. *J. Can. Pet. Technol.* **14** (1975).

18. N. R. Morrow, Wettability and Its Effect on Oil Recovery. *J. Pet. Technol.* **42**, 1–476 (1990).

19. R. I. Al-Raoush, Impact of Wettability on Pore-Scale Characteristics of Residual Nonaqueous Phase Liquids. *Environ. Sci. Technol.* **43**, 4796–4801 (2009).

20. A. AlRatrout, M. J. Blunt, B. Bijeljic, Wettability in complex porous materials, the mixed-wet state, and its relationship to surface roughness. *Proc. Natl. Acad. Sci.*, 201803734 (2018).

21. A. R. Kovscek, H. Wong, C. J. Radke, A Pore-Level Scenario for the Development of Mixed-Wettability in Oil Reservoirs. *AlChE JJournal* **39**, 58 (1992).

22. W. Barthlott, C. Neinhuis, Purity of the sacred lotus, or escape from contamination in biological surfaces. *Planta* **202**, 1–8 (1997).

23. X. Gao, *et al.*, The Dry-Style Antifogging Properties of Mosquito Compound Eyes and Artificial Analogues Prepared by Soft Lithography. *Adv. Mater.* **19**, 2213–2217 (2007).

24. T. Bultreys, *et al.*, Fast laboratory-based micro-computed tomography for pore-scale research: Illustrative experiments and perspectives on the future. *Adv. Water Resour.* **95**, 341–351 (2016).

25. P. J. Withers, *et al.*, X-ray computed tomography. *Nat. Rev. Methods Primer* **1**, 18 (2021).

26. S. Berg, *et al.*, Real-time 3D imaging of Haines jumps in porous media flow. *Proc. Natl. Acad. Sci.* **110**, 3755–3759 (2013).

27. T. Bultreys, *et al.*, Real-time visualization of Haines jumps in sandstone with laboratory-based microcomputed tomography. *Water Resour. Res.* **51**, 8668–8676 (2015).

28. K. Singh, *et al.*, Dynamics of snap-off and pore-filling events during two-phase fluid flow in permeable media. *Sci. Rep.* **7** (2017).

29. M. Rücker, *et al.*, From connected pathway flow to ganglion dynamics. *Geophys. Res. Lett.* **42**, 3888–3894 (2015).

30. C. A. Reynolds, H. Menke, M. Andrew, M. J. Blunt, S. Krevor, Dynamic fluid connectivity during steady-state multiphase flow in a sandstone. *Proc. Natl. Acad. Sci.* **114**, 8187–8192 (2017).

31. M. Rücker, *et al.*, The Effect of Mixed Wettability on Pore-Scale Flow Regimes Based on a Flooding Experiment in Ketton Limestone. *Geophys. Res. Lett.* **46**, 3225–3234 (2019).

32. A. Scanziani, Q. Lin, A. Alhosani, M. J. Blunt, B. Bijeljic, “Dynamics of displacement in mixed-wet porous media” (EarthArXiv, 2020) https:/doi.org/10.31223/osf.io/jpmvc (April 8, 2020).

33. S. Schlüter, S. Berg, T. Li, H.-J. Vogel, D. Wildenschild, Time scales of relaxation dynamics during transient conditions in two-phase flow: RELAXATION DYNAMICS. *Water Resour. Res.* **53**, 4709–4724 (2017).

34. N. Molenaar, “Origin of Low-Permeability Calcite-Cemented Lenses in Shallow Marine Sandstones and CaCO3 Cementation Mechanisms: An Example from the Lower Jurassic Luxemburg Sandstone, Luxemburg” in *Carbonate Cementation in Sandstones*, S. Morad, Ed. (Blackwell Publishing Ltd., 1998), pp. 193–211.

35. R. T. Armstrong, S. Berg, Interfacial velocities and capillary pressure gradients during Haines jumps. *Phys. Rev. E* **88**, 043010 (2013).

36. R. Lenormand, C. Zarcone, Role of roughness and edges during imbibition in square capillaries. *SPE J.* (1984).

37. K. Singh, T. Bultreys, A. Q. Raeini, M. Shams, M. J. Blunt, Imbibition in porous media: correlations of displacement events with pore-throat geometry and the identification of a new type of pore snap-off. 12 (2019).

38. A. Q. Raeini, B. Bijeljic, M. J. Blunt, Generalized network modeling: Network extraction as a coarse-scale discretization of the void space of porous media. *Phys. Rev. E* **96** (2017).

39. A. AlRatrout, A. Q. Raeini, B. Bijeljic, M. J. Blunt, Automatic measurement of contact angle in pore-space images. *Adv. Water Resour.* **109**, 158–169 (2017).

40. A. Mascini, V. Cnudde, T. Bultreys, Event-based contact angle measurements inside porous media using time-resolved micro-computed tomography. *J. Colloid Interface Sci.* **572**, 354–363 (2020).

41. T. Akai, Q. Lin, A. Alhosani, B. Bijeljic, M. Blunt, Quantification of Uncertainty and Best Practice in Computing Interfacial Curvature from Complex Pore Space Images. *Materials* **12**, 2138 (2019).

42. R. M. El-Maghraby, M. J. Blunt, Residual CO2 Trapping in Indiana Limestone. *Environ. Sci. Technol.* **47**, 227–233 (2013).

43. M. J. Blunt, *Multiphase Flow in Permeable Media: A Pore-Scale Perspective* (Cambridge University Press, 2017).

44. Q. Lin, *et al.*, Minimal surfaces in porous media: Pore-scale imaging of multiphase flow in an altered-wettability Bentheimer sandstone. *Phys. Rev. E* **99**, 063105 (2019).

45. T. Pak, I. B. Butler, S. Geiger, M. I. J. van Dijke, K. S. Sorbie, Droplet fragmentation: 3D imaging of a previously unidentified pore-scale process during multiphase flow in porous media. *Proc. Natl. Acad. Sci.* **112**, 1947–1952 (2015).

46. T. M. Aminabhavi, V. B. Patil, M. I. Aralaguppi, H. T. S. Phayde, Density, Viscosity, and Refractive Index of the Binary Mixtures of Cyclohexane with Hexane, Heptane, Octane, Nonane, and Decane at (298.15, 303.15, and 308.15) K. *J. Chem. Eng. Data* **41**, 521–525 (1996).

47. Y. Gao, Q. Lin, B. Bijeljic, M. J. Blunt, X-ray Microtomography of Intermittency in Multiphase Flow at Steady State Using a Differential Imaging Method. *Water Resour. Res.* **53**, 10274–10292 (2017).

48. K. Singh, *et al.*, Time-resolved synchrotron X-ray micro-tomography datasets of drainage and imbibition in carbonate rocks. *Sci. Data* **5** (2018).

49. A. L. Herring, A. Sheppard, L. Andersson, D. Wildenschild, Impact of wettability alteration on 3D nonwetting phase trapping and transport. *Int. J. Greenh. Gas Control* **46**, 175–186 (2016).

50. M. Khishvand, A. H. Alizadeh, M. Piri, In-situ characterization of wettability and pore-scale displacements during two- and three-phase flow in natural porous media. *Adv. Water Resour.* **97**, 279–298 (2016).

51. S. Van Offenwert, V. Cnudde, T. Bultreys, Pore-Scale Visualization and Quantification of Transient Solute Transport Using Fast Microcomputed Tomography. *Water Resour. Res.* **55**, 9279–9291 (2019).